Investigation of Magnetic and Antimagnetic Bands in Nuclei

Awad Kishore Singh[1], Dr. Vipin Kumar[2]

[1]Research Scholar, OPJS University, Churu Rajasthan
[2]Research Supervisor, OPJS University, Churu Rajasthan

Abstract

Using the Mossbauer effect, it was shown that the hyperfine field is generated in a direction opposite to the magnetization of the nonmagnetic Fe2+ ions, whose nuclei produce the field indirectly. So, in this essay, we looked at how the nanoparticle's dimensions, shape, doping, and coating affect its magnetic characteristics. We wrap off by discussing the current clinical position of magnetic nanoparticles in the study of magnetic fluid hyperthermia. Below the ferromagnetic transition temperature of TC = 220 K, we use both methods to take measurements with no applied field. First principles simulations are used to duplicate and explain the experimental data, proving the method's validity for quantitative estimates in alloys of technological importance.

Keywords: *magnetic multilayers, transition metal compounds, Mossbauer spectroscopy, magnetic ordering, crystal structure.*

1. INTRODUCTION

There have been a number of investigations into pyrites, or compounds with the MX2 structure (where M = Fe, Co, Ni,... and X = S, Se). The magnetic and electrical characteristics that these compounds display in combination are intriguing and need further study. Because of the low-spin arrangement of the Fe 2+ ions, FeS2 is a nonmagnetic semiconductor that displays only weak van Vleck paramagnetic behaviour as a function of temperature. CoS2, a close isostructural analogue, is likewise a ferromagnet (Tc = 120 K) with metallic conduction. Recent research has shown that the nuclei of nonmagnetic iron ions Fe 2+ substituted in COS2 generate a magnetic hyperfine field at temperatures below Tc'. However, a thorough theoretical investigation of the Mossbauer spectrum of Fe57 in COO. 98Feo.O2 at 91 K reported by Woodhams et al. was found to be challenging due to the mixing of the magnetic-dipole and electric-quadrupole interactions, which are of comparable magnitude. It turns out that there are two equally plausible sets of hyperfine (HF) interaction parameters that can be calculated from analytical modelling, depending on the sign of the electric quadrupole. Magnetic HF field direction could not be determined in either case. explained theoretically why the NMR frequency of the low-spin diamagnetic ion C03 + in compound C03 04 changes as a function of temperature. It was shown that the magnetic C0 2+ ions induce an HF field into the nucleus of the C03 + ion, thereby causing the transformation.

Because the C03 + ion in C0304 is isoelectronic with the Fe2+ ion in FeS2 and is also analogous to it in its spin state and the presence in both cases of constant temperature independent van Vlock paramagnetic moments, it was interesting to compare the mechanisms of the indirect HF interactions in C0304 and (COS2)O.97(FeS2)O.03'. Direct experimental determination of the sign of this field is crucial for a complete characterisation of these interactions. In addition, the published publications gave ideas on the angular spin structure of the C02 + ions in COS2. Investigating the HF interactions at the Fe S7 nuclei in (COS2)O.97(FeS2)O.03 at external magnetic fields up to 60 kore and temperatures spanning 4.2-135 K, this study aims to shed light on these puzzles.

Nuclear quadrupole resonance spectroscopy is used to identify substances having quadrupolar nuclei (QN). Ionization transitions between nuclear ground-state sublevels are produced and detected by subjecting the sample to powerful radiofrequency (RF) pulses, much as in nuclear magnetic resonance (NMR). To elaborate, NMR takes place when nuclei interact primarily with an external static magnetic field, whereas NQR takes place when nuclei interact primarily with electric field gradients (EFG) inside the material. It is only possible for quadrupole splitting to take place if the electric quadrupole moment of the nucleus is sufficiently big. The condition for this to be true is if the spin quantum number I is greater than 1/2. The EFG is a consequence of the interaction between the electric quadrupole moment of the nucleus and the non-spherical distribution of charges in its surrounds.

2. LITERATURE REVIEW

Gupta, Yogesh (2021) In this thesis, we explore nuclei with a nearly closed shell and few valence nucleons outside the magic-core. Because of the multiple mechanisms by which the high angular momentum associated with a wide range of nuclear structural phenomena can be generated in near closed shell nuclei, these nuclei are useful for the experimental testing of numerous theoretical theories. Primarily closed shell nuclei were studied here, including 104Pd, 145Eu, and 145Gd.

Vicky V. Mody (2013) The process of magnetic hyperthermia involves heating biocompatible, small-sized iron oxide nanoparticles using an alternating magnetic field (AMF), which may subsequently be utilised to enhance contrast in biological tissue. But the size, shape, surface flaws, and coatings of magnetic nanoparticles put limits on their behavior in a magnetic field. Conjugating a magnetic nanoparticle to a site-specific ligand or peptide is one of the most promising novel formulations of nanoparticles being investigated for tissue targeting at the moment, making it crucial to keep an eye on the nanoparticles' magnetic characteristics. So, in this essay, we looked at how the nanoparticle's dimensions, shape, doping, and coating affect its magnetic characteristics. Now that we've covered the background of magnetic fluid hyperthermia and the current clinical status of magnetic nanoparticles, we can wrap things up.

R. Hussain (2019) We report on Mn NMR experiments using a standard set of FeP-based MnFePSi samples, conducted in both zero and applied magnetic field. Truncated order parameter curves with a high value of the local ordered moment at the Curie point show the first-order nature of the magnetic transition, even in compositions where the transition seems second order from magnetic measurements. Complete ferromagnetic domains are discovered to be phase separated from volume fractions where Mn spins are fluctuating but weak ferromagnetic order is not detected at Si-poor compositions displaying the kinetic arrest phenomena. The mixed magnetism of these materials is shown to be created by a decline in the 3f spin density rather than enhanced spin fluctuations, as seen by a bigger fall in the ordered moment at the 3f sites than at the 3g sites on reaching TC. In accordance with theoretical predictions and in contrast to earlier observations, which only found a partial moment quenching, it is shown that the temperature-driven 3f spin extinction evolves into a completely nonmagnetic state of the 3f Mn ions well above TC. The disproportionation at 3f sites of a substantial minority Mn fraction with small hyperfine couplings, which retains its diamagnetic character regardless of temperature, may be detected by NMR in Mn-rich compositions. The decreased average 3f moment previously recorded at high Mn concentrations can be understood qualitatively as a result of the presence of such a diamagnetic component.

François Guillou (2014) MnFe materials have considerable temperature swings when placed in a magnetic field, but they also have minimal hysteresis and high mechanical stability. The latent heat observed at the Curie point may be regulated without affecting the magnetic characteristics of MnFe compounds by partly replacing B for P, which results in intriguing magnetocaloric features well-suited for magnetic refrigeration.

3. BASICS OF MAGNETISM: SOFT AND HARD MAGNETS

The term "magnetic materials" is used to describe a wide range of materials with magnetic properties. Their magnetic properties permit useful categorization. At room temperature, the magnetic properties of elements can be explained by diamagnetism and paramagnetic, the two most frequent forms of magnetic activity. As a result, A majority of the elements in the periodic table are not magnetic, but the few that are are classified as ferromagnetic. Ferromagnetism is the dominant magnetic phase in most materials of industrial significance.

The motion of charged and massive particles is typically responsible for magnetic phenomena. Electrons, holes, protons, and both positive and negative ions fall under this category. It is well known that in a ferromagnetic material, each magneton is a group of electrically charged particles spinning around each other, creating the magnetic dipole. Figure 1 further shows that the bulk of a ferromagnetic material is made up of many smaller regions of magnetons called domains. Walls between domains are the boundaries between them. Instead of thinking of these "domain walls" as mere surfaces, it is helpful to picture them as transitional regions of varying thicknesses, where the magnetization progressively shifts from one side to the other (Figure 1).

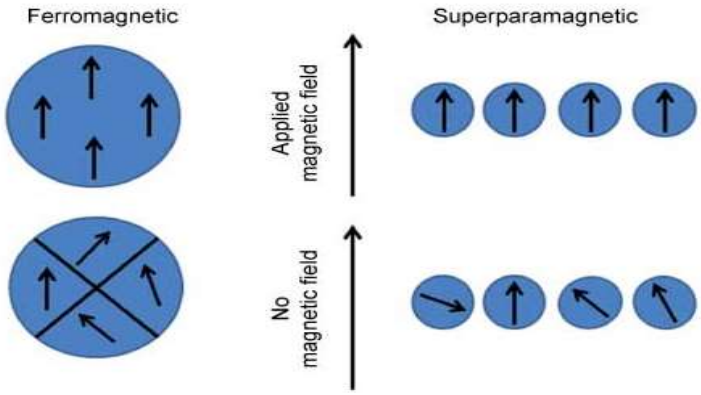

Figure 1

A magnetic moment is present in both ferromagnetic and superparamagnetic substances.

Therefore, in a ferromagnetic material, A magnetic domain is a region of a material in which the exchange forces have oriented all of the magnetons in the same direction. Separating ferromagnetic materials from paramagnetic ones, these domains. Because the magnetizations in magnetic domains are randomly oriented, ferromagnetic materials in their demagnetized condition have no magnetization. However, when an external magnetic field is applied, the magnetic domain boundaries are erased, and the magnetic moments align with the direction of the magnetic field, completely saturating the magnetization. (Figure 1). Saturation magnetization (Ms) refers to the highest level of magnetization that can be achieved (Figure 2). When a magnetic field is supplied to a ferromagnet and then withdrawn, the ferromagnet retains a memory of the field. However, a coercive force is required to totally remove the magnetism from a ferromagnetic substance. Consequently, coercivity is a method for evaluating the ability of a ferromagnetic material to resist demagnetization. Hysteresis is the name given to this phenomenon that occurs in ferromagnetic materials, and the route it follows is termed a hysteresis loop (Figure 2). What sets ferromagnets distinct from paramagnets is their hysteretic response to an applied magnetic field.

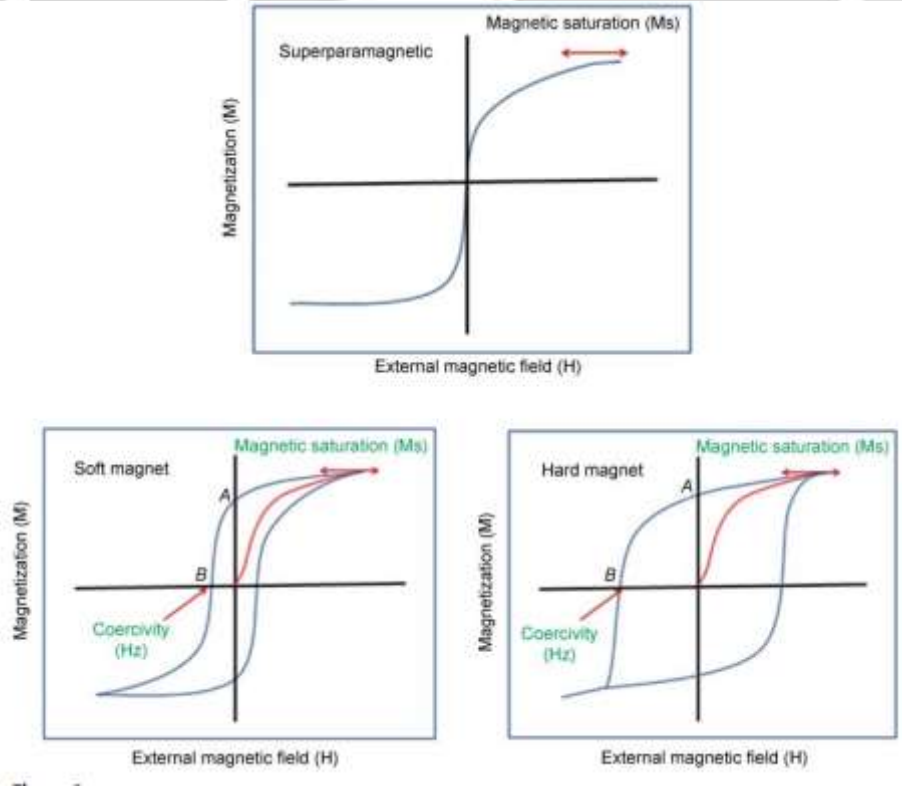

Figure 2: The hysteresis loop seen in both superparamagnetic and ferromagnetic materials is common.

As shown in Figure 2, ferromagnetic materials are divided into two types, "soft" and "hard" magnetic, based on their sensitivity to magnetic fields. Those magnetic materials with a low coercivity (Hc) are considered soft because they can be demagnetized in weak magnetic fields. Conversely, soft magnetic materials have high permeability because they can be magnetized readily. So, a low magneto crystalline anisotropy is one possible explanation for the effortless movement of magnetic domains in a soft ferromagnetic material. Differences in physical or mechanical qualities along distinct axes, such as magnetic susceptibility, absorbance, refractive index, conductivity, tensile strength, etc., are examples of anisotropy. For ferromagnetic materials, a larger magnetic field is needed to align the magnetic moments when the domain wall is difficult to migrate. Hard magnets are made from these ferromagnetic materials. So, it takes a lot of effort to magnetize these ferromagnetic materials, but once they are, it takes much more effort to unmagnetized them. Since soft magnetic materials lack magneto crystalline anisotropy and coercivity (Hc), it stands to reason that hard magnetic materials possess these features.

Hard ferromagnetic materials typically exhibit memory due to their inability to lose their magnetization when subjected to an applied magnetic field. Instead, soft ferromagnetic materials like iron or silicon steel are well-suited for use in a wide range of biomedical applications because their magnetic hysteresis loops are extremely tiny. There is also effort involved in closing the hysteresis loop, as coercive force must be provided to counteract the remaining magnetism. This magnetic hysteresis causes energy to be lost in the form of heat, with the amount of energy lost being directly proportional to the size of the magnetic hysteresis loop. Therefore, the extent of the loss is proportional to the coercive force value of the substance.

As a result, we can exploit the generated heat to our advantage by directly heating the tumor cells where they are located. There is a strong correlation between the type of magnetic material and its biological applications because heat loss is controlled by the hysteresis loop, which in turn is controlled by the magnetic material. To produce a temperature, increase of 5-10°C, for instance, a soft magnet is typically favored for usage in magnetic hyperthermia. Coercivity (Hc) is a measure of how strongly a material repels a magnet, and is thus crucial to determining which magnet will best serve a given purpose. Several parameters, including particle size and shape, defect concentration, surface effects, and temperature, all play a role in determining the ferromagnetic characteristics of a given material. The engineering of nanoparticles for biomedical applications is dependent on factors such as particle size, shape, and surface coatings, we have attempted to explore the influence of coercivity on these characteristics in the following section.

4. RESULTS

- **NMR**

At low temperatures, spontaneous ZF NMR signals were observed between 70 and 90 MHz and 13 and 24 MHz, respectively, roughly correlating with the frequency regions where analogous resonances were discovered and ascribed to 31P in P1 and P2 and 57Fe in Fe1 and Fe2 in their work. In Fig. The higher-frequency region of the ZF spectrum at 5 K is fitted by a multi-Gaussian distribution, as shown in Fig. 1(a). High frequency suggests that these resonances come from 31P nuclei, since a 57Fe resonance at the same frequency would correspond to hyperfine fields of 60 T, demanding an unphysical local moment >5 B according to the known iron hyperfine coupling. Shorter and significantly attenuated rf pulses were used to produce nuclear spin echoes in nonmagnetic materials, indicating a considerable rf increase of the resonance. When compared to the optimal excitation circumstances in a strong applied field that saturates the magnetization (see below), where 1 2 can be determined, the average enhancement factor was calculated to be on the order of 1000. Such a high value of demonstrates that these signals are generated by nuclei in domain walls .

As can be seen in Fig. 1(a), the 31P ZF spectrum displays a structure with two peaks at around 78 and 88 MHz. P2 and P1 were found to be the resonance peaks for such characteristics. However, experimental evidence contradicts such a conclusion. First, Two close-frequency peaks in a homogeneous magnetic structure cannot account for the factor-3 difference in enhancement factors for the two spectral characteristics, indicating nuclei at different places within a domain wall. The two-cusp structure progressively disappears under the magnetic saturation field. On the same diagram are shown the 31P nuclei 5 K spectra for the vast majority of domains.

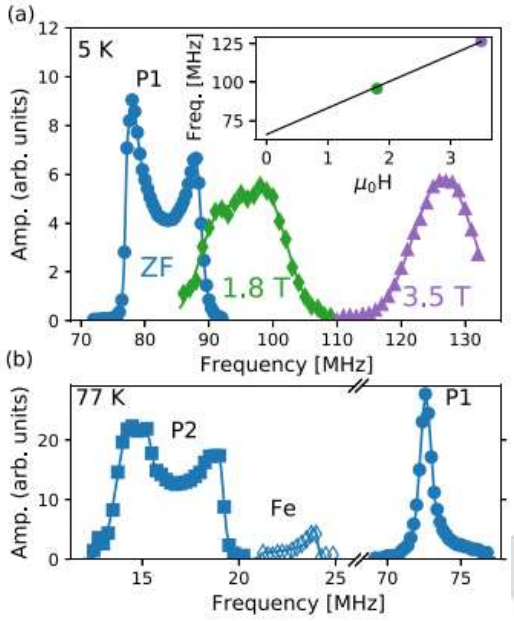

FIG. 1. Portions of the spectra containing just noise are omitted for clarity.

Magnetic moment of polycrystalline Fe2P is almost saturated at 0H = 1.8 T and nearly fully saturated at 0H = 3.5 T. Consistent with 31P nuclei with a positive hyperfine coupling, the resonance frequency varies from H to H as a result of the vector composition of the internal field with the external field as v = = 0(H H) 31/2, and the lineshape tends to a single Gaussian curve when the field strength is increased. This set of NMR readings indicates a single resonance line, P1, as determined by the DFT calculations detailed below. The unusual lineshape of the ZF spectrum at 5 K is likely due to the anisotropic component of the hyperfine coupling and the particular micromagnetic structure of domain walls, in which spins within a wall do not sample the solid angle with equal probability.

Full magnetization of the polycrystalline sample, on the other hand, allows for random sampling of angles independent of crystal axes. The rms anisotropic hyperfine field Banis exp = 3 2/31 = 0.46(1) T is the result of a spectral linewidth of = 4.6 MHz in the larger applied field. Although the isotropic hyperfine field at this point may be estimated using the first moment of the spectrum, B(iso) hf = 2/31 = 4.7(1) T, this result is erroneous owing to the absence of knowledge about the structure of the domain walls. Due to the linear dependency of the resonance frequency on the applied fi eld strength, the average weighted by the multi-Gaussian fit in Fig. 1 offers a different estimate B(iso) hf = 2(0)/31 = 3.83 (4) T is the result of the fit shown in the inset of the same figure, in which parameter (0) is left unconstrained. The 31P1 ZF spectrum transforms into a single smaller peak when the temperature is raised, and is once again represented by a phenomenological multi-Gaussian fit. It is calculated that the spectral width is = 1.1(1) MHz at 77.3 K, and that the two-cusp structure has totally disappeared, leaving just the primary peak at 72.6 MHz and a weaker Gaussian shoulder. Two decades of experiments have shown that the amplitude of rf pulses has no effect on the form of the 77.3 K spectrum, which indicates a shift in the anisotropic hyperfine coupling. By comparing it to spectra collected under different spin-echo excitation settings, this was established.

From 5 to 77.3 K, P1's anisotropic hyperfine coupling diminishes, leading to a narrowing of the ZF spectrum. A smooth order parameter curve for the mean resonance frequency vs temperature is obtained when the system is heated further; up to 160 K, the (T) values are in good agreement with the literature. NMR loses signal too quickly at that temperature for the magnetic transition to be studied. These lower-frequency resonances seen in Fig. 1(b) were investigated at a temperature of 77.3 K. When examining NMR spectra of ZF, you'll see an asymmetric peak at 23.7 MHz and a broader, more intense composite line between 14 and 18 MHz. The latter figure is in excellent agreement with the 17.2 T hyperfine field observed by 57Fe Mössbauer spectroscopy for Fe2 at the same temperature. The evidence presented here is consistent with the identification of 57Fe as the element corresponding to this NMR line.

However, the other larger resonance is not consistent with the 57Fe NMR of Fe1, despite the fact that the identical Mössbauer data predicts such a resonance line at 15.0 MHz (Bhf = 10.9 T). Since there is an equal number of Fe atoms in both sites, the integrated amplitude of the two signals should be the same. The 14-18 MHz signal must originate from the 31P resonance in a mean spontaneous field of 0.94(4) T at the

complementary P2 site, since this line is significantly more sensitive than the 57Fe(1) line. Different from the original literature, our assignment may be confirmed by measuring the relative sensitivity of the two nuclear species: R = R Bhf = a 3B3 hf = a 3. Nuclear sensitivity, R, is proven to be proportional to the local field B and the abundance an in a nonmagnetic material by the equation R = a 3B2, but in a ferromagnet, the sensitivity additionally relies on B = Bhf owing to the enhancement factor. After adjusting for spectrum size, we found that the ratio of 31Rn/57Rn = 11 is in good agreement with the value of 31A/57A 16 that we calculated experimentally. Compared to apples and oranges, it's like apples and pears, but better. Due to the enormous discrepancy in the amplitudes of the 31P NMR resonances between protons.

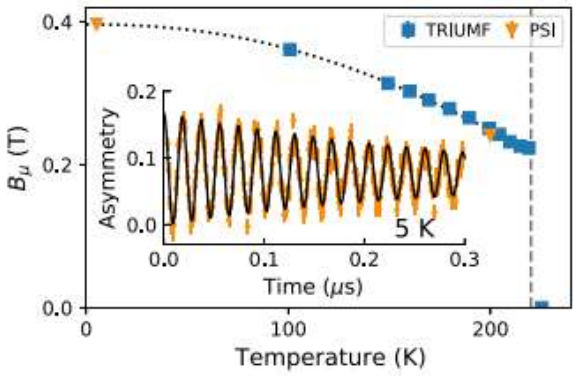

FIG. 2. The local field at the muon site as a function of temperature extracted from fits to ZF-μSR data collected at TRIUMF and PSI.

When comparing the 5 K 31P1 spectrum to the 77.3 K 31P2 spectrum, comparable arguments may be made for both. We estimate its linewidth to be v = 1.8(1) MHz and its P2 rms anisotropic hyperfine field to be Banis exp = 3 2/31 = 0.18(1) T, making it substantially bigger than the comparable P1 values at the same temperature. Our findings provide a framework for the interpretation of future studies on Fe2P alloys of technological relevance, and they show that theory and experiment are in great accord.

5. CONCLUSION

that the C02+ moments in COS2 are arranged in a spiral pattern. Because of the collinear structure, the saturation moment per C02+ ion is just 0.84 ilB instead of the 1 ilB predicted by theory, we can assume the angle between the moments has a value of 25°, as proposed in the angular spin structure is described within the context of the itinerant-electron model by the partial overlap of the magnetic sub-bands of itinerant d -electrons with spin up and spin down, leading to a reduction in the measured moment. The experimental linewidth is found to be highly correlated with the strength of the magnetic HF field, as shown by preliminary computer calculations (with a fixed angle). Since magnetic dipole and electric quadrupole interactions are intertwined, it stands to reason that the thickness of the absorber must be taken into account while analyzing such spectra. Research aimed at answering these concerns is ongoing. The study of magnetic hyperthermia has advanced to the clinical stage; in the future, it may be possible to use hyperthermia to treat malignancies as a quick, outpatient procedure with few complications.

6. REFERENCES

1. Gupta, Yogesh K.; Sahu, R.R.; Santra, S.; Gupta, A.K. (Nuclear Physics Division, Bhabha Atomic Research Centre, Mumbai (India)) (eds.); Board of Research in Nuclear Sciences, Department of Atomic Energy, Mumbai (India); [977 p.]; Dec 2021; [2 p.]; 65. DAE-BRNS symposium on nuclear physics; Mumbai (India); 1-5 Dec 2021; Article No. TA3
2. Mody, Vicky V., Singh, Ajay and Wesley, Bevins. "Basics of magnetic nanoparticles for their application in the field of magnetic fluid hyperthermia" European Journal of Nanomedicine, vol. 5, no. 1, 2013, pp. 11-21. https://doi.org/10.1515/ejnm-2012-0008
3. R. Hussain, F. Cugini, S. Baldini, G. Porcari, N. Sarzi Amadè, X. F. Miao, N. H. van Dijk, E. Brück, M. Solzi, R. De Renzi, and G. Allodi, Phys. Rev. B 100, 104439 (2019)
4. F. Guillou, Sun-Liting, O. Haschuluu, Z. Ou, E. Brück, O. Tegus, and H. Yibole, J. Alloys Compd. 800, 403 (2019).
5. L. Caron, M. Hudl, V. Höglin, N. H. Dung, C. P. Gomez, M.Sahlberg, E. Brück, Y. Andersson, and P. Nordblad, Phys. Rev. B 88, 094440 (2013).

6. N. H. Dung, Z. Q. Ou, L. Caron, L. Zhang, D. T. C. Thanh, G. A. de Wijs, R. A. de Groot, K. H. J. Buschow, and E. Brück, Adv. Energy Mater. 1, 1215 (2011)
7. Zhuravlev, V. P. Antropov, A. Vishina, M. van Schilfgaarde, and K. D. Belashchenko, Phys. Rev. Materials 1, 051401(R) (2017).
8. Carlsson, M. Gölin, and S. Rundqvist, J. Solid State Chem. 8, 57 (1973).
9. Scheerlinck and E. Legrand, Solid State Commun. 25, 181 (1978).
10. H. Fujii, S. Komura, T. Takeda, T. Okamoto, Y. Ito, and J. Akimitsu, J. Phys. Soc. Jpn. 46, 1616 (1979).
11. J. Tobola, M. Bacmann, D. Fruchart, S. Kaprzyk, A. Koumina, S. Niziol, J.-L. Soubeyroux, P. Wolfers, and R. Zach, J. Magn. Magn. Mater. 157-158, 708 (1996).
12. Koumina, M. Bacmann, D. Fruchart, J. Soubeyroux, P. Wolfers, J. Tobola, S. Kaprzyk, S. Niziol, M. Mesnaoui, and R. Zach, Ann. Chim. Sci. Mater. 23, 177 (1998).
13. H. Fujii, Y. Uwatoko, K. Motoya, Y. Ito, and T. Okamoto, J. Phys. Soc. Jpn. 57, 2143 (1988).
14. X. F. Miao, L. Caron, J. Cedervall, P. C. M. Gubbens, P. Dalmas de Réotier, A. Yaouanc, F. Qian, A. R. Wildes, H. Luetkens, A. Amato, N. H. van Dijk, and E. Brück, Phys. Rev. B 94, 014426 (2016).
15. N. H. Dung, L. Zhang, Z. Q. Ou, L. Zhao, L. van Eijck, A. M. Mulders, M. Avdeev, E. Suard, N. H. van Dijk, and E. Brück, Phys. Rev. B 86, 045134 (2012)